Optimal LLC Inverter Design with SiC MOSFETs and Phase Shift Control for Induction Heating Applications

Vicente Esteve, *Senior member, IEEE,* José Jordán, *Senior member, IEEE,* Esteban Sanchis-Kilders, *Senior member, IEEE,* Enrique J. Dede, *Member, IEEE,* Pedro J. Martinez, Enrique Maset, *Member, IEEE,* David Gilabert

***Abstract* – This work presents the analysis of a converter based on an LLC resonant output inverter and its optimal design used in induction heating applications. The new optimal design method improves several operating parameters that leads to an optimization of the dimensioning of the components of the converter. Additionally, this converter achieves an output power factor that can be considered optimal since it allows to minimize the reactive power of the resonant circuit components and reduces the rms values of the output current of the inverter and the current of its switching devices in relation to that found in traditional designs. A complete study of the circuit based on classic models is carried out to introduce simple rules for the design of this type of inverter for induction heating applications and to control its output power based on a phase shift system (PS). Since the inverter is made with silicon carbide (SiC) MOSFET transistors, an efficiency greater than 99% is reached. The experimental results were obtained from the test of a 12 kW 20 kHz converter for induction heating application.**

Index terms: Power converters. LLC inverters Induction Heating. SiC power MOSFETs. PS power control.

I. INTRODUCTION

THE basic induction heating converters are based on resonant inverters in which the load circuit is formed by the heating coil, its equivalent loss resistance, and a series capacitor, in a series resonant inverter (SRI) [1] - [3] or in parallel, in a parallel resonant inverter (PRI) [4] - [7]. Both are used for heating, welding, melting, hardening, and more metal heat treatment applications.

The use of series resonant converters, which are fed with a voltage source, represents a cost-effective solution since they normally use a pulse frequency modulation (PFM) [8] [9], a phase shift (PS) [10] [11] or a pulse density modulation (PDM) [12] [13] to regulate the output power using a diode bridge rectifier as an unregulated DC voltage source. SRI may need a transformer for matching the output power and high current in the induction coil. Parallel resonant inverters can achieve high inductor currents without a matching transformer but for PRI simple power control strategies are not usually easily applicable and they normally use a rectifying converter at their input that acts as an adjustable current source and an inverter, made up of bidirectional voltage and unidirectional current switches, adjusted to work very close to resonance. All this makes PRI inverters too complex circuits.

To solve these PRI difficulties, a modification of the parallel resonant circuit is proposed by adding an auxiliary series inductance, which the results in an LLC resonant circuit. Previous work has shown that the LLC resonant inverter maintains PRI properties using a simple DC input voltage source and power control strategies easily achievable that provide short circuit immunity [9]. However, the connection of the inductance in series (L_S) with the parallel resonant circuit generates an additional phase shift which must be optimized to minimize the reactive power of the resonant circuit components reducing the output current of the inverter and the switching current of its switching devices.

On the other hand, traditional LLC inverters are built using silicon (Si) IGBT or MOSFET switches. The developed inverter uses SiC-MOSFET technology as per its superior characteristics over Si-IGBT. When comparing the same chip area, for a 1000 V Si and 6H-SiC devices, the last one has a current density 20.6 times higher than Si and the specific on resistance is 305.7 times lower for the 6H-SiC device than for the Si device [24]. Switching losses are much lower in SiC devices than in Si ones, making these components ideal as HF switches. Other advantages of SiC over Si are their high temperature operation capability and its controlled avalanche behaviour.

The article is organized as follows: section II presents the properties of the LLC resonant circuit, section III shows the configuration and operation of the LLC inverter, while section IV gives a design method that optimizes the selection of the components of the inverter. In section V a practical design of an industrial induction heating application is carried out with which the feasibility of the approximations made can be verified. Section VI introduces the phase-shift based power

Manuscript received April 14, 2021; revised July 6, 2021; accepted October 7, 2021. Date of publication xxxx xx, xxxx. (Corresponding author: Vicente Esteve)

Vicente Esteve, José Jordán, Esteban Sanchis-Kilders, Enrique Maset and David Gilabert are with the Electronic Engineering Department, University of Valencia, Burjassot, 46100, Spain. (E-mail: vesteveg@uv.es; jose.jordan@uv.es; esteban.sanchis@uv.es; emaset@uv.es; david.gilabert@uv.es).

Enrique J. Dede and Pedro Martínez are with SiCtech Induction, Paterna, 46980, Spain. (E-mail: edede@sictechinduction.com; pmartinez@sictechinduction.com).

Color versions of one or more of the figures in this article are available online at https://ieeexplore.ieee.org.

Digital Object Identifier xxxxxxxxxxxxxxxxxxx.

control system, analysing its operation, conducting a power loss study, and proposing a control circuit. Section VII shows the experimental results. Finally, the conclusions drawn from the work are presented.

II. The LLC resonant circuit

The LLC resonant circuit is composed of three reactive components, two inductors and a capacitor (LLC) and the equivalent load resistance connected as shown in Fig. 1.

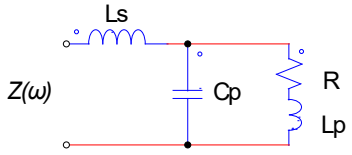

Fig. 1. LLC resonant circuit.

In topological terms it can be considered that the LLC circuit is a series-parallel hybrid since it behaves at the input as a current source, like a series resonant circuit, and at the output as a voltage source as occurs in parallel resonant circuits. Therefore, it is to be expected that it will maintain some of the most advantageous characteristics of each of these circuits. The LLC circuit will be connected to a voltage-fed inverter which simplifies the configuration of the input section of the converter, like an SRI, and the current through the output inductor will be amplified if we work close to parallel resonance as in a PRI, which can prevent the installation of current step-up transformers.

The input impedance $Z(\omega)$ of the circuit can be written as:

$$Z(\omega)=L_p\,\omega_o(\beta+1)\frac{\frac{1}{Q}\left[\frac{1}{\beta+1}-\left(\frac{\omega}{\omega_o}\right)^2\right]+j\frac{\omega}{\omega_o}\left[1-\left(\frac{\omega}{\omega_o}\right)^2\right]}{\left[1-\left(\frac{\omega}{\omega_{op}}\right)^2\right]+j\frac{\omega}{Q_p\omega_{op}}} \quad (1)$$

where ω is the operating angular frequency. The resonant angular frequency of the parallel resonant circuit is:

$$\omega_{op}=\frac{1}{\sqrt{L_pC_p}} \quad (2)$$

and its quality factor is defined by:

$$Q_p=\frac{L_p\omega_{op}}{R} \quad (3)$$

The ratio between the inductances is

$$\beta=\frac{L_s}{L_p} \quad (4)$$

The resonant angular frequency of the LLC circuit is:

$$\omega_o=\frac{1}{\sqrt{L_{eq}C_p}}=\frac{1}{\sqrt{(L_s\,\|\,L_p)C_p}}=\sqrt{\frac{\beta+1}{\beta}}\cdot\omega_{op} \quad (5)$$

Q is the quality factor of the heating inductor is:

$$Q=\frac{L_p\omega_o}{R}=\sqrt{\frac{\beta+1}{\beta}}\cdot Q_p \quad (6)$$

At resonance the input impedance of the resonant circuit can be expressed as [9]:

$$Z(\omega_o)=\frac{L_p\,\omega_o\beta^2}{Q-j(\beta+1)} \quad (7)$$

and its argument is:

$$\varphi=\arg(Z(\omega_o))=\arctan\left(\frac{\beta+1}{Q}\right) \quad (8)$$

The current gain $H_i(\omega)$ is the relationship between the heating inductor current $i_o(\omega)$ and the input current of the resonant circuit $i(\omega)$ (see Fig. 3) which can be expressed as:

$$H_i(\omega)=\frac{i_o(\omega)}{i(\omega)}=\frac{v_o(\omega)/(R+jL_p\omega)}{v_o(\omega)/((R+jL_p\omega)\,\|\,(1/jC_p\omega))}=$$
$$=\frac{1}{1-\left(\frac{\omega}{\omega_{op}}\right)^2+j\frac{\omega}{Q_p\omega_{op}}} \quad (9)$$

At resonance, and combining the last two equations, we have:

$$\left|H_i(\omega_o)\right|=\frac{\beta}{\sqrt{1+\left(\frac{\beta+1}{Q}\right)^2}}=\beta\cos\varphi \quad (10)$$

This means that the current gain of the LLC circuit is greater the lower the phase of the impedance. For small phases the gain can be approximated to $H_i(\omega_o)=\beta$.

Fig. 2 shows the graphical representation of the main quantities that describe the LLC circuit as a function of ω.

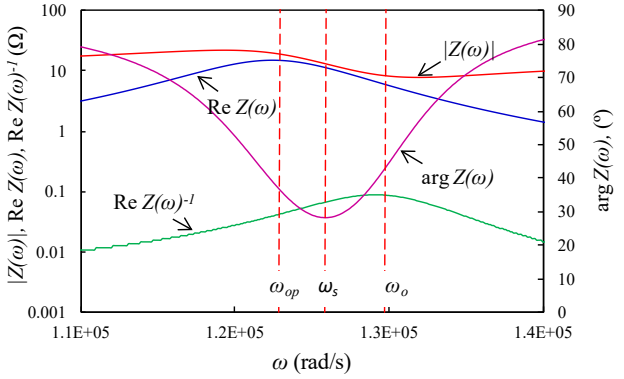

Fig. 2. Impedance module (red), impedance argument (magenta), real part of impedance (blue) and real part of admittance (green) of the circuit resonant LLC.

Observing these graphs, the following can be concluded:

- The real part of the impedance has its maximum at the parallel resonant frequency ω_{op}.
- The real part of the admittance has its maximum at the equivalent resonant frequency ω_o.
- There is a minimum in the impedance argument at a frequency ω_s between the two frequencies above.

From the analysis of the operation of the circuit in these three points, it can be deduced what the optimal operating point should be. Working near ω_{op} , the maximum output power would be obtained if we feed the circuit with a current source which is not our case, since the topologically correct inverter must be powered by a voltage source. Near ω_o the maximum power is obtained when the circuit is supplied with a voltage

source. This is the usual choice [9], but it has several drawbacks. The phase is relatively large and this makes the inverter current values (rms and switching) high. Furthermore, the operating point is not easy to find by simple control techniques.

However, when operating near the minimum of the impedance argument, an optimal output power factor is achieved and, as the input impedance is higher, the circuit currents will be lower than when operating at ω_o. This allows a smaller dimensioning of the components of the inverter. The rms values of the current of the inverter and the switching current of its switches will have a minimum value for a given output power and an improvement of the inverter efficiency will be reached. Furthermore, under these conditions the current gain of the resonant circuit is maximized. It should be noted that this is only possible as long as the sign of the argument is positive in order to guarantee inductive type switching and thus ensuring smooth ON switching. These facts will be verified experimentally at the end of this article.

III. THE LLC RESONANT INVERTER

Fig. 3 shows the LLC inverter configuration consisting of a complete inverter bridge powered by direct voltage and an LLC resonant circuit connected to its output.

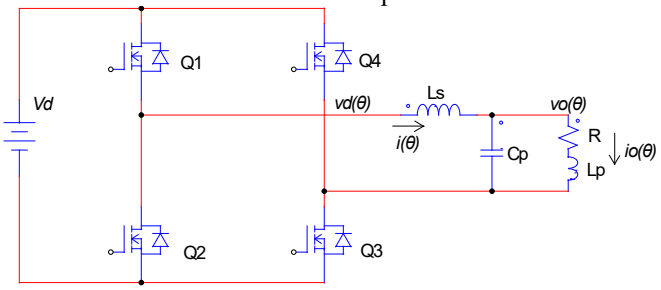

Fig. 3. LLC resonant inverter.

For sufficiently high values of Q_p the output voltage $v_o(\theta)$ has an approximated sinusoidal value:

$$v_o(\theta) = V_p \sin(\theta) \tag{11}$$

where V_p is the peak value of $v_o(\theta)$. Therefore, the circuit can be reduced to the one shown in Fig. 4.

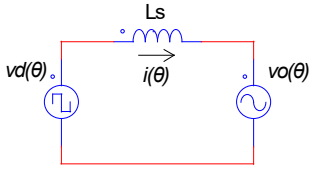

Fig. 4. Equivalent Circuit of Resonant Inverter LLC.

Analysing the circuit of Fig. 4 the following equation can be written:

$$v_d(\theta) - v_o(\theta) = L_s \frac{d}{dt} i(\theta) \tag{12}$$

where $v_d(\theta)$ can be written as:

$$v_d(\theta) = \begin{cases} V_d & \text{if} \quad \gamma - \pi < \theta < \gamma \\ -V_d & \text{if} \quad \gamma < \theta < \gamma + \pi \end{cases} \tag{13}$$

where γ is the phase of the inverter commutation with respect to the phase origin of the output voltage.

Integrating (12) and solving the integration constants in order to have a continuous function, we obtain:

$$i(\theta) = \begin{cases} \dfrac{V_d}{L_s \omega}\left(\theta + n\cos(\theta) + \dfrac{\pi}{2} - \gamma\right) & \text{if} \quad \gamma - \pi \le \theta \le \gamma \\ \dfrac{-V_d}{L_s \omega}\left(\theta - n\cos(\theta) - \dfrac{\pi}{2} - \gamma\right) & \text{if} \quad \gamma \le \theta < \gamma + \pi \end{cases} \tag{14}$$

where $n = V_p/V_d$. The corresponding waveforms are shown in Fig. 5.

An approximation to the minimum value of phase shift would be obtained when the value of the current at the moment of commutation is the smallest possible. In this case, the time necessary to discharge the inductance L_S to zero will be minimal and therefore also the phase shift between voltage and current. This condition will be fulfilled when the output voltage in the commutation $v_o(\gamma)$ is equal to V_d, which allows us to introduce the equation:

$$\gamma = \pi - \arcsin\left(\frac{1}{n}\right) \tag{15}$$

Hence, the switching current will be:

$$I_c = \frac{V_d}{L_s \omega}\left(n\cos(\gamma) + \frac{\pi}{2}\right) \tag{16}$$

and the peak current will be calculated by making $\theta = \pi - \gamma$.

$$I_p = \frac{V_d}{L_s \omega}\left(2(\pi - \gamma) - n\cos(\gamma) - \frac{\pi}{2}\right) \tag{17}$$

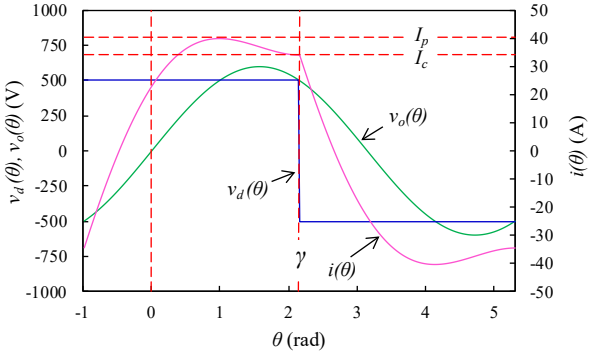

Fig. 5. Waveforms of the LLC resonant inverter. The blue curve corresponds to the output voltage, the magenta one to the output current and the green one to the voltage of the parallel resonant circuit.

Since the value of I_C must be positive (inductive commutation), the range of variation of n allowed is:

$$1 < n < \frac{\sqrt{\pi^2 + 4}}{2} \tag{18}$$

IV. RESONANT LLC INVERTER DESIGN

In order to design the components of the output circuit and obtain the values of amplitudes and phases of currents and voltages of the inverter, we have to start by calculating the active output power of the inverter.

$$P_o = \frac{1}{2\pi}\int_0^{2\pi} i(\theta) v_d(\theta) d\theta = \frac{V_d^2}{L_s \omega \pi}\int_{\gamma-\pi}^{\gamma}\left(\theta + n\cos(\theta) + \frac{\pi}{2} - \gamma\right) d\theta$$

$$P_o = \frac{2V_d^2}{\pi L_s \omega} \tag{19}$$

Therefore, the value of the series inductance is calculated with:

$$L_s = \frac{2V_d{}^2}{\pi P_o \omega} \tag{20}$$

The working frequency can be obtained taking into account the value of the phase angle [12] from equation:

$$\omega = \frac{\omega_{op}\left(\tan(\alpha)+\sqrt{\tan^2(\alpha)+4Q_p{}^2}\right)}{2Q_p} \tag{21}$$

Since in induction heating the values of Q_p are usually high, always greater than 5, the approximation $\tan^2(\alpha) << 4Q_p{}^2$ can be made and, in that case, applying (15), (21) can be approximated to:

$$\omega = \frac{\omega_{op}\left(\frac{\pi n^2}{4}-\sqrt{n^2-1}+2Q_p\right)}{2Q_p} \tag{22}$$

The values of the rest of the components of the resonant circuit can be easily obtained by means of the following equations if we suppose that the working frequency is close enough to the resonance:

$$R_p = \frac{V_p{}^2}{2P_o} \tag{23}$$

where $R_p=Q_p{}^2R$ is the parallel equivalent resistance of the parallel resonant circuit at resonance.

$$C_p = \frac{2Q_pP_o}{\omega V_p{}^2} \tag{24}$$

$$L_p = \frac{1}{\omega^2 C_p} \tag{25}$$

Keep in mind that the value of the first harmonic of the current is:

$$i_1(\theta) = I_1 \sin(\theta+\alpha) \tag{26}$$

where the amplitude and phase of this first harmonic is obtained from the following equations:

$$I_1{}^2 = \left[\frac{2}{\pi}\int_{\gamma-\pi}^{\gamma}\frac{V_d}{L_s\omega}\left(\theta+n\cos(\theta)+\frac{\pi}{2}-\gamma\right)\cos(\theta)d\theta\right]^2 + \left[\frac{2}{\pi}\int_{\gamma-\pi}^{\gamma}\frac{V_d}{L_s\omega}\left(\theta+n\cos(\theta)+\frac{\pi}{2}-\gamma\right)\sin(\theta)d\theta\right]^2 \tag{27}$$

$$\alpha = \arctan\frac{\int_{\gamma-\pi}^{\gamma}\frac{V_d}{L_s\omega}\left(\theta+n\cos(\theta)+\frac{\pi}{2}-\gamma\right)\cos(\theta)d\theta}{\int_{\gamma-\pi}^{\gamma}\frac{V_d}{L_s\omega}\left(\theta+n\cos(\theta)+\frac{\pi}{2}-\gamma\right)\sin(\theta)d\theta} \tag{28}$$

Integrating and applying (15) we obtain:

$$I_1 = \frac{V_d}{L_s\omega}\frac{\sqrt{(\pi n)^2-8\pi\sqrt{n^2-1}+16}}{\pi} \tag{29}$$

$$\alpha = \arctan\left(\frac{\pi n^2}{4}-\sqrt{n^2-1}\right) \tag{30}$$

On the other hand, the values of the amplitude and phase of the first harmonic of the input voltage to the circuit can be obtained by means of the following equations:

$$V_{d1} = \frac{4}{\pi}V_d \tag{31}$$

$$\lambda = \gamma - \pi \tag{32}$$

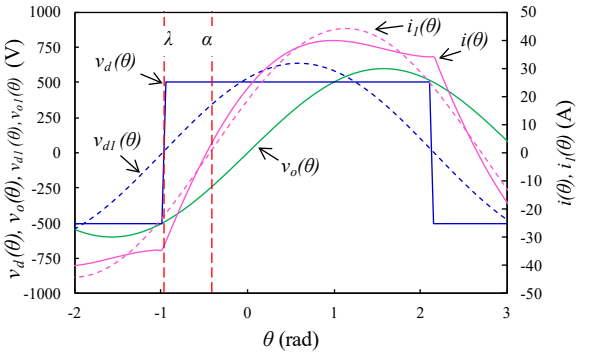

Fig. 6. Waveforms of the LLC resonant inverter (solid lines) and their first harmonics (dashed lines). The blue curves correspond to the output voltage, the magenta ones to the output current and the green one to the voltage of the parallel resonant circuit.

Fig. 6 shows the waveforms of the circuit voltages and currents and their corresponding first harmonics. It can be deduced that the phase between the input voltage and current of the resonant circuit, that is, the phase of the input impedance at the working frequency, can be approximated to the following value:

$$\varphi = \alpha - (\gamma - \pi) \tag{33}$$

which is a positive value since the impedance shows an inductive behaviour for the working frequency.

V. Comparative Design Example

In this section, a design of the components and magnitudes of the inverter is made using the equations of the previous section for a practical case whose specifications are summarized in Table I.

TABLE I
DESIGN SPECIFICATIONS

Magnitude	Symbol	Value	Unit
Output power	P_o	12	kW
Quality factor	Q_p	10	
Switching frequency	f_s	20	kHz
Output peak voltage	V_p	600	V
DC input voltage	V_d	500	V

Table II shows the results obtained by applying the corresponding equations from previous sections.

TABLE II
RESULTS OF THE OPTIMAL DESIGN

Magnitude	Symb.	Eq.	Value	Unit
Parallel frequency	f_{op}	22	19.54	kHz
Series frequency	f_o	5	20.64	kHz
Equivalent resistance	R_p	23	15	Ω
Parallel capacitor	C_p	24	5.43	μF
Parallel inductor	L_p	25	12.22	μH

Series inductor	L_S	20	105.5	µH
First harmonic current	I_1	29	44.2	A
Switching current	I_C	17	34.2	A
Output V, I phase	φ	33	31.3	º
Current gain	$\|H_i\|$	10	8.56	

The graphical representation of the main quantities that describe the LLC circuit of this design example as a function of ω was shown in Fig. 2. It is observed that the minimum of the phase is sufficiently close to that calculated in equation (33). This fact determines the viability of the assumptions and approximations made, thus validating the design method, where we find an operation point that corresponds to a minimum value of the phase difference between the inverter output voltage and current.

Table III shows the result of the design using traditional methods working on the resonance frequency [9] for the same starting specifications.

TABLE III
RESULTS OF THE CLASSIC DESIGN

Magnitude	Symb.	Value	Unit
Series inductor	L_S	127.3	µH
First harmonic current	I_1	54.6	A
Switching current	I_C	58.8	A
Output V, I phase	φ	49.4	º
Current gain	$\|H_i\|$	6.94	

All values have been improved using the proposed design method. Fig. 7 shows the percentage value of each parameter in Table III with respect to those in Table II. Enhanced output current, series inductance, and output phase shift optimize component sizing, efficiency and cooling requirements.

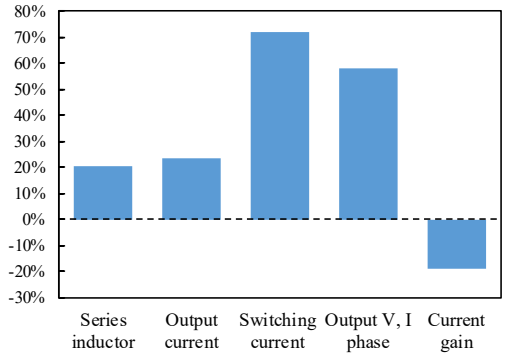

Fig. 7. Percentage value of each parameter in Table III with respect to those in Table II

VI. PHASE-SHIFT POWER CONTROL

Nowadays, voltage source resonant inverters are widely used in applications that require output power control capability using a variety of control methods. In pulse frequency modulation (PFM), the output power can be controlled by varying the switching frequency while the inverter operates under a zero voltage switching (ZVS) scheme. Hybrid control methods [14]-[17] and asymmetrical duty-cycle control [18] are also used for LLC resonant converters.

In traditional LCC inverter designs the maximum output power is obtained by operating at the resonance frequency ω_o. As the operating frequency increases, the module and argument of the input impedance of the LLC circuit increases so the output power decreases. This is not possible for our design where we have to keep the inverter working near the minimum of the input impedance of the resonant circuit for any output power. The solution to regulate the output power in our design is to use a phase-shift modulation.

The phase-shift (PS) control technique varies the output power by shifting the phase of the switches conduction sequence [19]-[21]. Fig. 8 shows the voltage waveforms applied to the LLC resonant circuit, and the gate drive voltages for the transistors of the bridge. The phase-shift between the two legs of the bridge corresponds to ϕ that varies from 0 to π. With phase-shift control, the rms of the voltage applied to the resonant tank varies and, hence, the output power.

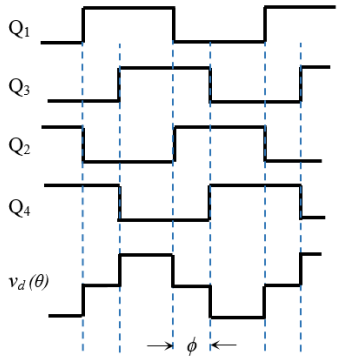

Fig. 8. Phase shift operation.

By means of this power control method, all circulating currents, both positive and negative, pass through the channel of the MOSFET transistors, which remain on for a complete half-cycle of the trigger sequence except for the dead time necessary to avoid the simultaneous conduction of transistors of the same branch. During this dead time the current goes through the freewheel diodes that are subsequently cut off in soft turn-on conditions. With the use of SiC MOSFET transistors, which have a high switching speed, the dead time can be reduced to values less than 100 ns. All the results and calculations presented in this section are based on the design of the previous section. Now the new equations of $v_d(\theta)$ and $i(\theta)$ can be written as:

$$v_d(\theta)=\begin{cases} 0 & \text{if} \quad \gamma-\pi<\theta<\gamma-\pi+\phi \\ V_d & \text{if} \quad \gamma-\pi+\phi<\theta<\gamma \\ 0 & \text{if} \quad \gamma<\theta<\gamma+\phi \\ -V_d & \text{if} \quad \gamma+\phi<\theta<\gamma+\pi \end{cases} \tag{34}$$

$$i(\theta)=\begin{cases} \dfrac{V_d}{L_s\omega}\left(n(\phi)\cos(\theta)-\dfrac{\pi-\phi}{2}\right) & \text{if} \quad \gamma-\pi\le\theta\le\gamma-\pi+\phi \\ \dfrac{V_d}{L_s\omega}\left(\theta+n(\phi)\cos(\theta)+\dfrac{\pi-\phi}{2}-\gamma\right) & \text{if} \quad \gamma-\pi+\phi\le\theta\le\gamma \\ \dfrac{V_d}{L_s\omega}\left(n(\phi)\cos(\theta)+\dfrac{\pi-\phi}{2}\right) & \text{if} \quad \gamma-\pi\le\theta\le\gamma+\phi \\ \dfrac{V_d}{L_s\omega}\left(-\theta+n(\phi)\cos(\theta)+\dfrac{\pi+\phi}{2}+\gamma\right) & \text{if} \quad \gamma+\phi\le\theta<\gamma+\pi \end{cases} \tag{35}$$

Both equations coincide with (13) and (14) for the case of $\phi = 0$. The value of n is now not constant since V_p decreases as the rms value of v_d decreases because of the phase shifting. Therefore, for a fixed working frequency, n is:

$$n(\phi) = n\cos\left(\frac{\phi}{2}\right) \tag{36}$$

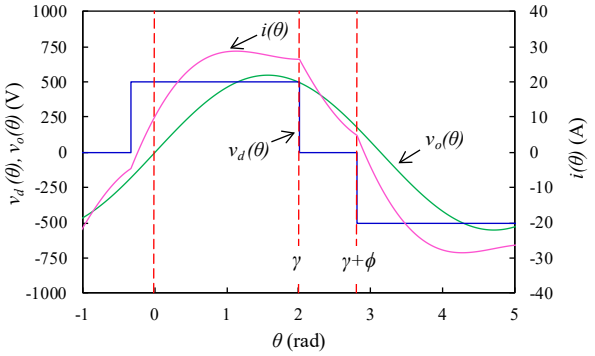

Fig. 9. Waveforms of the LLC resonant inverter with PS. The blue curve corresponds to the inverter output voltage, the magenta one to the output current and the green one to the voltage of the parallel resonant circuit.

The waveforms corresponding to equations (34) and (35) are shown in Fig. 9. For transistor Q_1 and, equivalently, for Q_4 the waveforms are shown in Fig. 10.

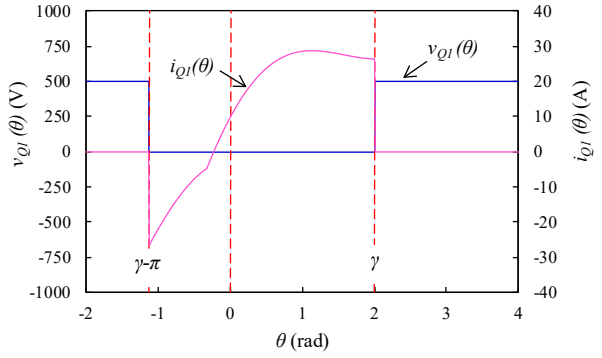

Fig. 10. Waveforms of the LLC resonant inverter with PS control. The blue colour curve corresponds to the drain-sourced voltage of Q_1, and the magenta one to the Q_1 current.

The switching currents for Q_1 and Q_4 are given by:

$$I_{cQ1}(\phi) = \frac{V_d}{L_s\omega}\left(n(\phi)\cos\gamma + \frac{\pi-\phi}{2}\right) \tag{37}$$

For transistor Q_3 and, equivalently, for Q_2 the waveforms are shown in Fig. 11.

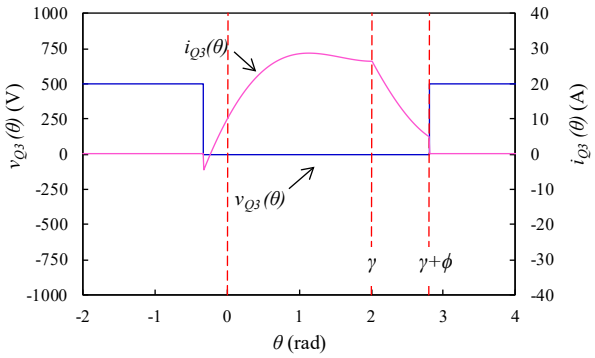

Fig. 11. Waveforms of the LLC resonant inverter with PS control. The blue colour curve corresponds to the drain-sourced voltage of Q_3, and the magenta one to the Q_3 current.

In this case the switching currents for Q_3 and Q_2 are lower due to the phase shift and are given by:

$$I_{cQ3}(\phi) = \frac{V_d}{L_s\omega}\left(n(\phi)\cos(\gamma+\phi) + \frac{\pi-\phi}{2}\right) \tag{38}$$

To maintain soft commutation, the condition that $I_{cQ3}(\phi)$ is always positive must be met, which leads to the following inequality that makes phase γ also depending on phase ϕ:

$$\gamma(\phi) \geq \arccos\left(\frac{\phi-\pi}{2n(\phi)}\right) - \phi \tag{39}$$

This means that the definition of phase $\gamma(\phi)$ must be calculated using the following piecewise function:

$$\gamma(\phi) = \begin{cases} \pi - \arcsin\left(\dfrac{1}{n(\phi)}\right) & \text{if} \quad n(\phi) > 1 \\ \arccos\left(\dfrac{\phi-\pi}{2n(\phi)}\right) - \phi & \text{if} \quad n(\phi) \leq 1 \end{cases} \tag{40}$$

Fig. 12 shows the evolution of $n(\phi)$ and $\gamma(\phi)$ according to equations (36) and (40) for V_d = 500 V and an initial value of V_p = 600 V when ϕ = 0.

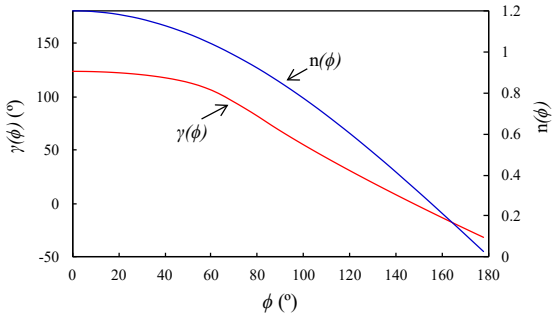

Fig. 12. Phase of turn-off switching and relationship between output and input voltage of the resonant circuit as a function of phase shift.

A. Output power

The calculation of the output power is carried out from the following equation obtained analogously to (18):

$$P_o = \frac{V_d^2 n(\phi)\left[\sin(\gamma(\phi)+\phi) + \sin(\gamma(\phi))\right]}{2\pi^2 L_s\omega} \tag{41}$$

Fig. 13 shows the evolution of the inverter output power as a function of the phase shift.

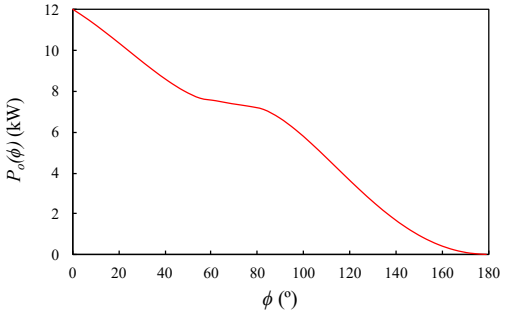

Fig. 13 shows the evolution of the inverter output power as a function of the phase shift.

B. Losses and efficiency analysis.

An efficiency analysis has been carried out considering the contribution of conduction (P_{cd}) and switching losses (P_{sw}) to total losses (P_{tot}) [22]. For the analysis of P_{sw}, we will only take into account the turn-off losses of the inverter bridge transistors because the turn-on switching losses are negligible. To

calculate the conduction losses, we need to previously calculate the rms value of the output current that can be approximated, for the sake of simplicity of the calculations, to the rms value of its first harmonic.

$$I_{rms}(\phi)=\frac{V_d\sqrt{4\cos(\phi)+(\pi\, n(\phi))^2+2\pi\, n(\phi)\left(\cos(\gamma(\phi)+\phi)+\cos\gamma(\phi)\right)+4}}{L_s\omega} \quad (42)$$

To compute the turn-off switching losses, we need compute (37) and (38). Fig. 14 shows graphically the currents indicated above.

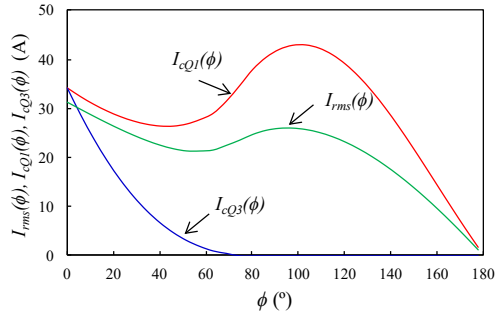

Fig. 14. Evolution of the turn-off switching currents and the rms values of the output current as a function of the phase shift.

Note that while the condition of (39) is maintained, the rms current decreases with increasing phase shift. However, when this condition cannot be met, the rms value of the current increases due to the change in working conditions imposed by ensuring the soft switching condition. Furthermore, under these conditions the switching current increases even more since the turn-off switching occurs at the peak of the current, which has a high crest factor.

Taking into account that the rms value of the current is the same for all the switches, the conduction losses can be calculated with the following equation.

$$P_{cd}(\phi)=\left(\frac{I_{rms}(\phi)}{\sqrt{2}}\right)^2 R_{DSon} \quad (43)$$

The transistor chosen for each of the inverter bridge switches is the SiC MOSFET C3M0032120K of V_{DS} = 1200 V and R_{DSon} = 32 mΩ. Based on the graphs of the turn-off switching energy E_{off} given by the manufacturer for a switching voltage of 600 V and a gate resistance of 2.5 Ω, it is possible to find the following polynomial function.

$$E_{off}(\phi)=a\, I_c^{\,2}+b\, I_c+c \quad (44)$$

where I_c is the switching current and a = 0.0546, b = -1.7479 y c = 37.8. Hence, the switching turn-off losses can be calculated.

$$P_{sw}(\phi)=E_{off}(\phi)f \quad (45)$$

For Q_1 and Q_4, switching power losses P_{swQ1} can be calculated from (45) introducing the switching current I_{cQ1} in (44). Analogously for Q_3 y Q_2 switching power losses P_{swQ3} are calculated with I_{cQ3}. To calculate the total power losses, we use the next equation.

$$P_{tot}(\phi)=4P_{cd}(\phi)+2\left(P_{swQ1}(\phi)+P_{swQ3}(\phi)\right) \quad (46)$$

The efficiency of the inverter can be calculated using the following expression.

$$\eta(\phi)=\frac{P_o(\phi)}{P_o(\phi)+P_{tot}(\phi)} \quad (47)$$

Fig. 15 shows the results of this loss analysis. It is clearly appreciated that the switching losses are reduced due to the use of SiC MOSFET transistors especially indicated for high frequency applications. Transistors Q_1 and Q_4 have more switching losses than transistors Q_2 and Q_3. For applications with a high number of thermal cycles, the reliability of the converter is reduced due to the phenomenon of power cycling. This fact can be improved by using an appropriate switching sequence [23].

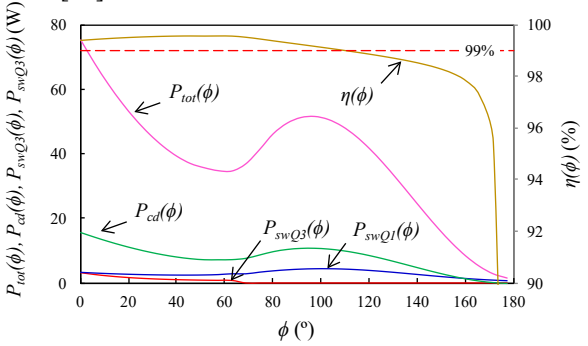

Fig. 15. Evolution of the power losses and the efficiency of the inverter as a function of the phase shift.

The most important losses at the chosen working frequency are those of conduction that always occur through the conduction channel of the MOSFET, whether they are direct or inverse currents. Efficiency is greater than 99% in a wide range of power output. For phase shifts close to 90º, an increase in conduction losses is observed due to the increase in the rms value of the current. Performance is penalized in this case but still remains above 98%.

C.LLC inverter control circuit

Fig. 16 shows the simplified schematic of the control circuit for the LLC inverter proposed in the previous sections. The main power control loop (Power regulation) manages the phase shift modulator (PS) that generates the trigger signals of transistors Q_3 and Q_4. The voltage controlled oscillator (VCO) tracks the frequency of the resonant circuit and generates the trigger signals of transistors Q_1 and Q_2. A phase detector (Phase detector) ensures, once the control loop is stabilized, that the phase between its X and Y inputs is near to zero. These inputs are the outputs of a logic circuit (logic inverter) whose two outputs are selected alternately between its inputs A and B depending on the logic value of signal C. The inputs to the logic circuit are the trigger signal of transistor Q_2 and a logic signal that is high when the current of Q_2 is positive. In stationary mode the control acts so that the transistor trigger signal is in phase with the positive part of its current, which ensures a soft turn-on switching of the transistor.

The minimum phase detector circuit manages the phase control loop to get the inverter to work near the minimum phase of the input impedance. This occurs when:

$$\frac{d\varphi}{d\omega}=\frac{d\varphi}{dt}\cdot\frac{dt}{d\omega}=\frac{d\varphi}{dt}\div\frac{d\omega}{dt}=0 \quad (48)$$

The digital output of the minimal phase detector circuit controls the logic inverter circuit to keep the inverter operating around the minimum phase of the input impedance of the resonant circuit.

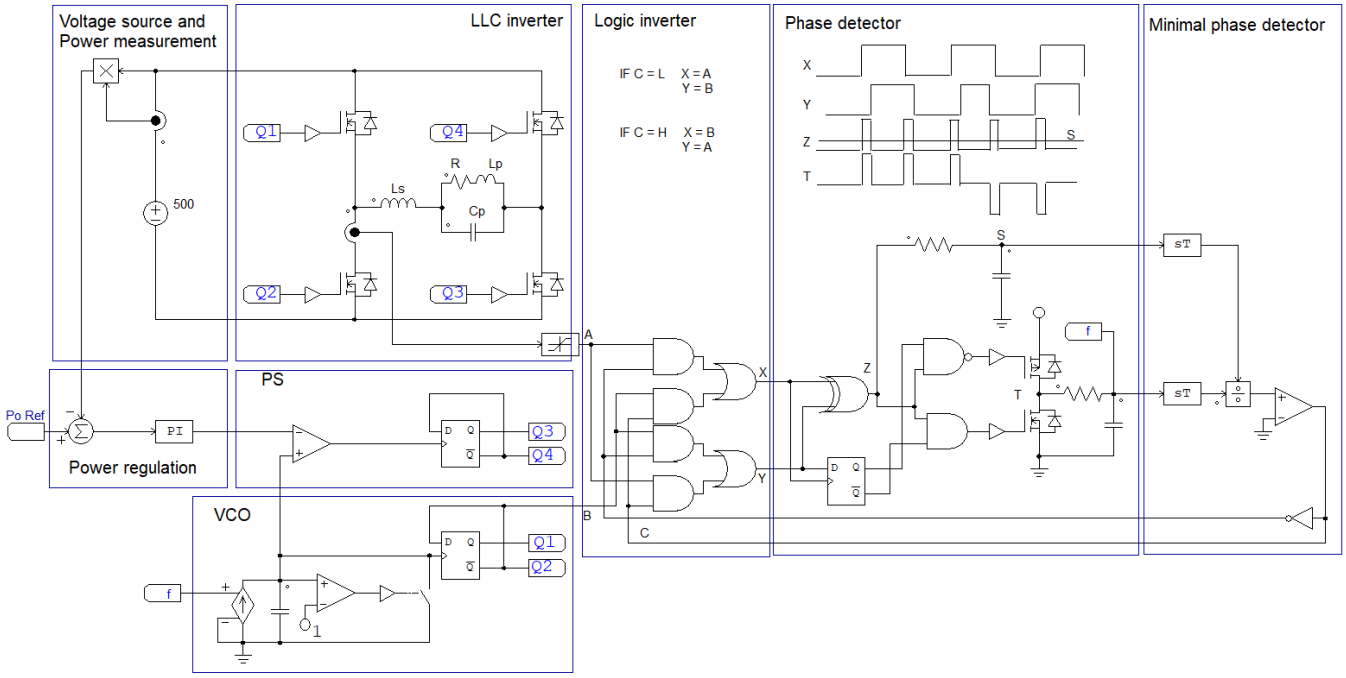

Fig. 16. Control diagram.

The value of the reactive components of the resonant circuit can change with temperature, especially the heating inductor L_p, whose value is modified by changes in magnetic permeability and electrical conductivity of the workpiece during the heating process. For this reason, the inverter control has a frequency tracking circuit and a minimum phase control circuit that achieve continuous feedback during inverter operation, maintaining the established conditions regardless of temperature. Note that if the control circuit assure the compliance of (48) the inverter works at the frequency where the impedance phase is minimum in any conditions and, hence, the frequency tracking is guaranteed.

To guarantee the safe operation of the inverter with low loads during start up, it is necessary to perform a frequency sweep starting from high values and large values of phase shifts, progressively decreasing both values until the stability of the power regulation is reached. In addition, the control circuit has protections that guarantee the reliable operation of the inverter in the event of overvoltages, overcurrents or sudden changes in working conditions such as a short-circuit situation in the heating inductor.

The main functions of the control circuit are carry out using a SmartFusion2 SoC field programmable gate array (FPGA). For the digital conversion of analogue signals and transistors triggering, we have chosen isolated delta-sigma modulators and drivers. The output of these circuits is separated from the input circuitry by a capacitive double isolation barrier that is highly resistant to magnetic interference. This barrier is certified to provide reinforced isolation and a very high transient immunity (>100 kV/μs). Used in conjunction with isolated power supplies, these isolated circuits separate parts of the system that operate on different common mode voltage levels and protects lower-voltage parts from damage.

VII. Experimental Results

This section shows the experimental results that have been obtained through the tests carried out on a 12 kW power prototype working at a frequency of around 20 kHz. The inverter was powered by a 500 V DC voltage source. The values of the components of the resonant circuit are approximately those obtained in section V. For the experimental verification, a test bed has been made composed of the following elements:

A. A Complete inverter bridge with four SiC C3M0032120K MOSFETs with an integrated digital electronic control on an FPGA-based system mounted on a water cooling heatsink.
B. A series inductor of 110 μH wound with Litz wire.
C. A high-power capacitor of 6 μF usable for induction heating.
D. A water-cooled solenoidal heating inductor of 12 μH.
E. A water-cooled test load to allow long-term tests.

Fig. 17 shows a picture of the test bed used to obtain the following experimental results.

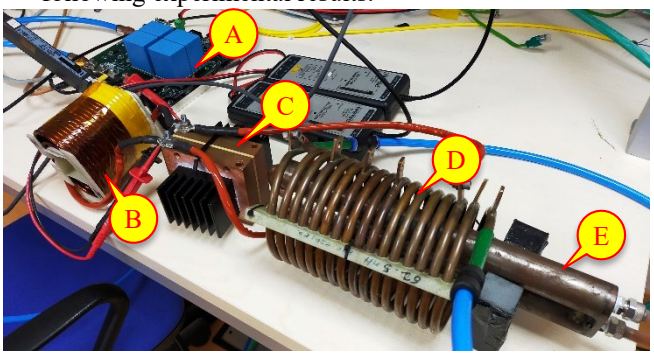

Fig. 17. LLC inverter test bed. Labels indicate items listed above

Fig. 18 shows DSO measurements of the main waveforms of the LLC inverter operating at full power. The expected output voltage and power values have been obtained although, due to the dispersion of the real values of the components with respect to those designed in section V, the switching frequency was 19 kHz. Fig. 19 shows DSO measurements of the main waveforms of the LLC inverter operating at medium power whit $\phi = 40º$ approximately.

Analyzing Fig. 18 and Fig. 19, the output voltage and current waveforms and peak current and switching current values measured in the experimental waveforms it can be confirmed that they are very close to the calculated values.

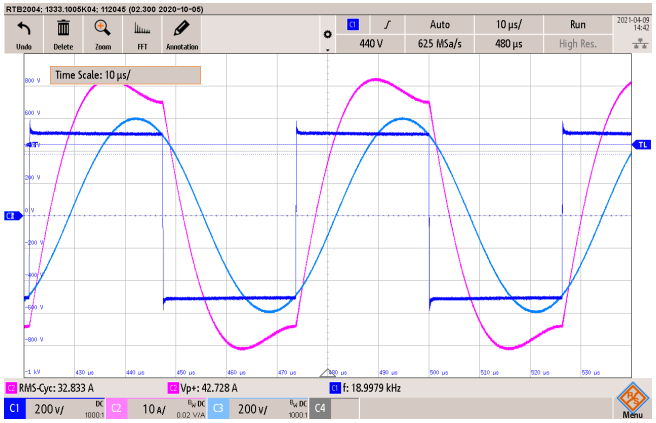

Fig. 18. Experimental waveforms of the LLC inverter for full power. C1 (dark blue) is the output voltage (200V/div), C2 (magenta) is the output current (10A/div) and C3 (light blue) is the inductor voltage (200V/div). Time base is 10 µs/div.

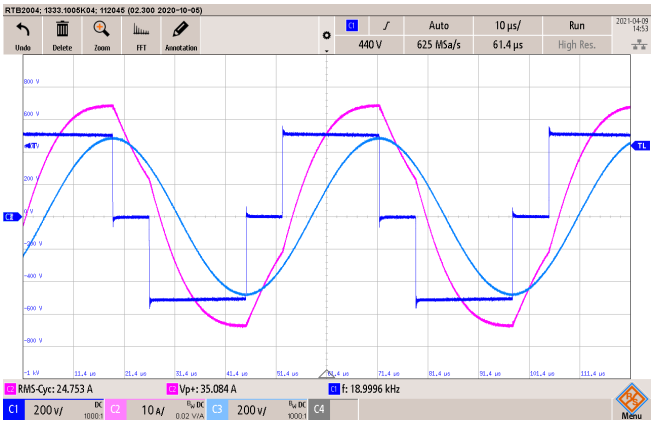

Fig. 19. Experimental waveforms of the LLC inverter for medium power. C1 (dark blue) is the output voltage (200V/div), C2 (magenta) is the output current (10A/div) and C3 (light blue) is the inductor voltage (200V/div). Time base is 10 µs/div.

Fig. 20 shows the graphs corresponding to the experimental measurements of the output power and efficiency of the LLC inverter bridge as a function of phase shift compared with the results of the calculations found in section VI. The output power was obtained by DSO measurement of the main value of the instantaneous multiplication of the output voltage and current of the inverter bridge. The input power was measured directly in the input DC voltage supply.

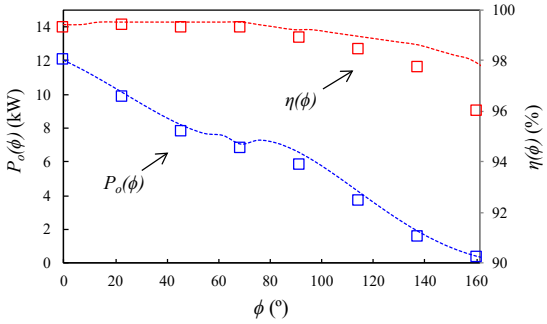

Fig. 20. Experimental output power and efficiency of LLC inverter in function of phase shift. Dashed lines represent the calculations and squares symbols are the experimental measurements.

Note that there are some differences between the experimental and calculated results that may be due to the modelling method used, the existence of losses of other elements not taken into account in the calculation (conductors, parasitic components, voltage and current sensors, etc.) and also to the measurement process.

Fig. 21 shows a thermal image of the prototype. This image will better support the efficiency measurements. Hottest points correspond to the current measurement circuits (shunt and current transformer).

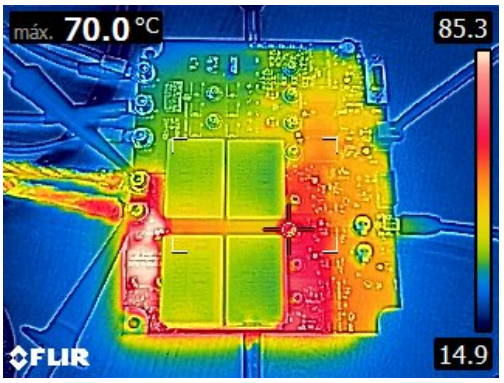

Fig. 21. Experimental output power and efficiency of LLC inverter in function of phase shift.

In order to check the optimality of the design with respect to classical design methods, the inverter was configured to switch close to the resonance frequency of the circuit while maintaining the same output voltage and power. Fig. 22 shows the waveforms obtained in this test. Under these conditions, it can be observed that the rms value of the inverter output current is 18 % higher and the switching current is 71 % higher. Note that the results are very close to those predicted in Fig. 7.

Finally, to confirm the feasibility of the design, comparative efficiency measurements between the design presented in this paper and the traditional one [9] working on the resonance frequency with PFM and PS power control, have been carried out. Fig. 23 shows experimental and calculated data in three cases. Since the power regulation is based on diferent variables, the horizontal axis of the graph must show a magnitude common to all designs, which in this case is the inverter ouput power.

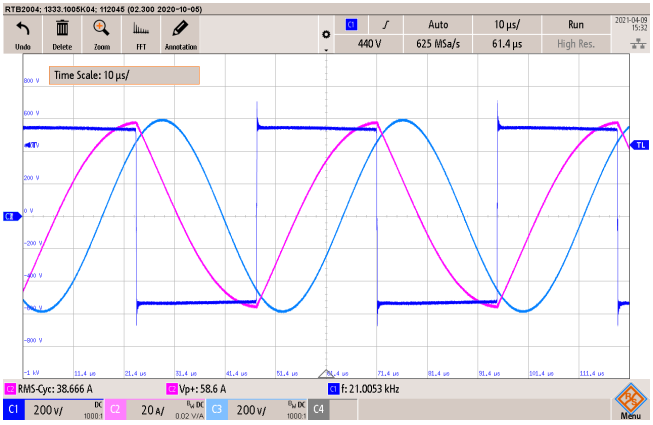

Fig. 22. Experimental waveforms of the classic LLC inverter for full power switching close to resonance frequency. C1 (dark blue) is the output voltage (200V/div), C2 (magenta) is the output current (20A/div) and C3 (light blue) is the inductor voltage (200V/div). Time base is 10 µs/div.

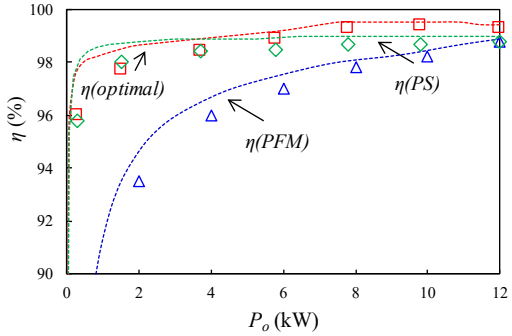

Fig. 23. Comparison between the efficiency of optimal design (red) and traditional design with PFM (blue) and PS (green) power control. Dashed lines represent the calculations and symbols are the experimental measurements.

VIII. Conclusions

In this work, a procedure has been shown that allows the design of LLC resonant inverters in a systematic way that makes it possible to choose optimally the reactive components and the switching frequency. This method permits to find a working point that corresponds to a minimum value of the phase difference between the inverter's output voltage and current. This means that, for certain specifications of power, frequency, output voltage and load factor Q, a design can be obtained that will present less current stress on the components of the resonant circuit, conductors and switches of the circuit while minimizing conduction and switching losses, and maximizing the efficiency of the converter. An inverter output power control technique based on PS modulation has also been presented. As a final test that gives viability to this design, more theoretical calculations and tests have been carried out comparing our results with those obtained in classic LLC inverter designs working near the resonance frequency with PFM power control. These have not been shown completely in this article which has a limited extension and will be presented in future articles.

References

[1] N.-J. Park, D.-Y. Lee, and D.-S. Hyun, "A power-control scheme with constant switching frequency in class-d inverter for induction-heating jar application," IEEE Trans. Ind. Electron., vol. 54, no. 3, pp. 1252–1260, Jun. 2007.

[2] S. Faucher, F. Forest, J.-Y. Gaspard, J.-J. Huselstein, C. Joubert, and D. Montloup, "Frequency-synchronized resonant converters for the supply of multiwinding coils in induction cooking appliances," IEEE Trans. Ind. Electron., vol. 54, no. 1, pp. 441–452, Feb. 2007.

[3] P. Savary, M. Nakaoka, and T. Maruhashi, "A high-frequency resonant inverter using current-vector control scheme and its performance evaluations," IEEE Trans. Ind. Electron., vol. IE-34, no. 2, pp. 247–256, May 1987.

[4] E. Dede, J. Gonzalez, J. Linares, J. Jordan, D. Ramirez, and P. Rueda, "25-kW/50-kHz generator for induction heating," IEEE Trans. Ind. Electron., vol. 38, no. 3, pp. 203–209, Jun. 1991.

[5] A. Shenkman, B. Axelrod, and V. Chudnovsky, "Assuring continuous input current using a smoothing reactor in a thyristor frequency converter for induction metal melting and heating applications," IEEE Trans. Ind. Electron., vol. 48, no. 6, pp. 1290–1292, Dec. 2001.

[6] D. W. Tebb and L. Hobson, "Design of matching circuitry for 100-kHz MOSFET induction heating power supply," IEEE Trans. Ind. Electron., vol. IE-34, no. 2, pp. 271–276, May 1987.

[7] K. B. Zhao, P. C. Sen, and G. Premchandran, "A thyristor inverter for medium-frequency induction heating," IEEE Trans. Ind. Electron., vol. IE-31, no. 1, pp. 34–36, Feb. 1984.

[8] L. A. Barragán, D. Navarro, J. Acero, I. Urriza, J. M. Burdío. "FPGA implementation of a switching frequency modulation circuit for emi reduction in resonant inverters for induction heating appliances," IEEE Trans. Ind. Electron., vol. 55, no. 1, Jan. 2008.

[9] J.M. Espí, E.J. Dede, R. García-Gil, J. Castelló. "Design of the L-LC resonant inverter for induction heating based on its equivalent SRI," IEEE Trans. Ind. Electron., vol. 54, no. 6, Dec. 2007.

[10] Z. M. Ye, P. K. Jain, P. C. Sen, "Full-bridge resonant inverter with modified PSM for HFAC power distribution systems," IEEE Trans. Ind. Electron., vol. 54, no. 5, Oct. 2007.

[11] S. Mollov, M. Theodoridis, and A. Forsyth, "High frequency voltage-fed inverter with phase-shift control for induction heating," Proc. Inst. Electr. Eng.—Electric Power Application, vol. 151, no. 1, pp. 12–18, Jan. 2004.

[12] H. Fujita and H. Akagi, "Pulse-density-modulated power control of a 4kW 450kHz voltage-source inverter for induction melting applications," IEEE Trans. Industry Appli., vol. 32, no.2, pp. 279-286, Mar.-Apr.1996.

[13] V. Esteve, E. Sanchis-Kilders, J. Jordan, E.J. Dede, C. Cases, E. Maset, J.B. Ejea, A. Ferreres, "Improving the Efficiency of IGBT Series-Resonant Inverters Using Pulse Density Modulation", IEEE Trans. Industrial Electronics, vol. 58, no. 3, pp. 979-987, 2011.

[14] J. Yamamoto, T. Zaitsu, S. Abe, and T. Ninomiya, "PFM and PWM hybrid controlled LLC converter," in Proc. IEEE Int. Power Electron. Conf., 2014, pp. 177–182.

[15] H.-P. Park and J.-H. Jung, "PWM and PFM hybrid control method for LLC resonant converters in high switching frequency operation," IEEE Trans. Ind. Electron., vol. 64, no. 1, pp. 253–263, Jan. 2017.

[16] N. Ahmed, "High frequency soft switching AC conversion circuit with dual mode PWM/PDM control strategy for high power IH applications," IEEE Trans. Ind. Electron., vol. 58, no. 4, pp. 1440–1448, Apr. 2011.

[17] J. Dudrik and N.-D. Trip, "Soft-switching PS-PWM DC–DC converter for full-load range applications," IEEE Trans. Ind. Electron., vol. 57, no. 8, pp. 2807–2814, Aug. 2010.

[18] S. Chudjuarjeen, A. Sangswang, and C. Koompai, "An Improved LLC Resonant Inverter for Induction-Heating Applications With Asymmetrical Control" IEEE Trans. Ind. Electron., vol 58, no. 7, pp. 2915-2925, Jul. 2011.

[19] Sabate, J.A., Jovanovic, M.M., Lee, F.C., Gean, R.T, "Analysis and design-optimization of LCC resonant inverter for high frequency AC distributed power system", IEEE Trans on Industrial Electronics, Volume 42, No. 1, Feb 1995, pp 63 -71, Feb 1995.

[20] Y. K. Lo, C. Y. Lin, M. T. Hsieh, and C. Y. Lin, "Phase-shifted full-bridge series-resonant DC–DC converters for wide load variations," IEEE Trans. Ind. Electron., vol. 58, no. 6, pp. 2572–2575, Jun. 2011.

[21] S. M. Showybul, Islam Shakib, and S. Mekhilef, "A frequency adaptive phase shift modulation control-based LLC series resonant converter for wide input voltage applications," IEEE Trans. Power Electron., vol. 32, no. 11, pp. 8360–8370, Nov. 2017

[22] O. Lucía, J. M. Burdío, I. Millán, J. Acero, and L. A. Barragán, “Efficiency oriented design of ZVS half-bridge series resonant inverter with variable frequency duty cycle control,” IEEE Trans. Power Electron., vol. 25, no. 7, pp. 1671–1674, Jul. 2010.
[23] V. Esteve, J. Jordan, E. Sanchis Kilders, E. Dede, E. Maset, J. Ejea, et al., "Improving the reliability of series resonant inverters for induction heating applications," IEEE Transactions on Industrial Electronics, vol. 61, pp. 2564-2572, May 2014.
[24] M. Bhatnagar and B. J. Baliga, "Comparison of 6H-SiC, 3C-SiC, and Si for power devices", IEEE Trans. Electron Devices, vol. 40, no. 3, pp. 645-655, Mar. 1993.

Vicente Esteve (M’03-SM’14) was born in Valencia, Spain, in 1961. He received the M.Sc. and Ph.D. degrees from the University of Valencia, Valencia, in 1986 and 1999, respectively.
He joined the Department of Electronic Engineering, University of Valencia, where he is currently an Associate Professor. His research activities include high-frequency rectifiers and inverters for industrial applications, high-power inverters for induction heating, and electronic instrumentation. He is a consultant to several electronics companies in the field of power supplies and advanced topologies. He has more than 20 years of experience on the design and testing of power electronic equipment.

José Jordán (M’08) was born in 1964. He received the M.Sc. degree in physics with specialization in electronics and the Ph.D. degree in electronics engineering from the University of Valencia, Burjassot, Spain, in 1989 and 2003, respectively.
From 1987 to 2001, he held research positions at GH Electrotermia, where his activities were focused on the design of high-frequency and high-power converters. He is currently an Assistant Professor with the University of Valencia. His research interests are power semiconductor characterization and power converters. In these areas, he is frequently a consultant to industrial concerns.
.

Esteban Sanchis-Kilders (M'00-SM'14) was born in Valencia, Spain, in 1967. He received the M.Sc. and the Ph.D. degree from the University of Valencia, Spain, in 1990 and 1997, respectively. After two years with the Power Conditioning Section of the European Space Agency (Noordwijk, The Netherlands) he joined the Laboratory of Industrial Electronics and Instrumentation of the University of Valencia in 1997, where he is now Full Professor. His main research interests are space power electronics, magnetism, control and industrial applications

Enrique J. Dede (M'95) received the Ph.D. degree in electronics from the University of Valencia, Valencia, Spain.
He is a Full Professor of Power Electronics at the University of Valencia and the Director of the company SiCtech Induction. He is the holder of several international patents on high-frequency inverters for induction heating and has written more than 250 papers in the field of power electronics. He has more than 25 years of experience in the design of high-power converters.
Dr. Dede is a member of the European Working Group of the IEEE Industry Applications Society and of the International Advisory Board of the PCIM-Europe and PCIM-China. He is a past President of the IEEE Spanish Joint Chapter of the Power Electronics Society and the Industrial Electronics Society. He is the Vice President of the European Power Electronics and Drives Association (EPE). He was the General Chair of EPE 2009 held in Barcelona, Spain.

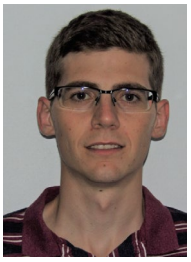

Pedro Martinez was born in Villarrobledo, Spain in 1992. He received the B.Sc. and M.S. degrees in electronic engineering in 2014 and 2015 respectively, from University of Valencia (Spain), where he is currently working toward the PhD. degree on reliability of GaN HEMT devices. Since 2018 is also a member of the the company SiCtech Induction. His research interest includes induction heating converters, the electronic power devices characterization and reliability and space power electronics.

Enrique Maset (M’00) was born in Xàtiva, Spain, in 1965. He received the M.Sc. and the PhD degree in physics, with specialization in electronics, from the University of Valencia, (Spain) in 1988 and in 1996, respectively. He is currently an Associate Professor in the Department of Electronic Engineering in the University of Valencia, where he is also a member of the Laboratory of Industrial Electronics and Instrumentation. His main research interests include space power electronics and static and dynamic characterization of electronic power devices.

David Gilabert was born in Alcoy, Spain, in 1984. He received the M.Sc. degree and the Ph. D. degree in Electronic Engineering from the University of Valencia, Spain, in 2014 and 2020, respectively. He is also a member of the Laboratory of Industrial Electronics and Instrumentation.
The research interests include high-frequency magnetics, coupled inductors and space power electronics.